Probing macroscopic quantum state with a sub-Heisenberg accuracy

Haixing Miao,[1] Stefan Danilishin,[2,3] Helge Müller-Ebhardt,[3] Henning Rehbein,[3] Kentaro Somiya,[4] and Yanbei Chen[4]

[1] *School of Physics, University of Western Australia, WA 6009, Australia*
[2] *Physics Faculty, Moscow State University, Moscow 119991, Russia*
[3] *Max-Planck Institut für Gravitationsphysik (Albert-Einstein-Institut) and Leibniz Universität Hannover, Callinstr. 38, 30167 Hannover, Germany*
[4] *Theoretical Astrophysics 130-33, California Institute of Technology, Pasadena, CA 91125, USA*

Significant achievements in the reduction of classical-noise floor will allow macroscopic systems to prepare nearly Heisenberg-Limited quantum states through a continuous measurement, i.e. conditioning. In order to probe the conditional quantum state and confirm quantum dynamics, we propose use of an optimal time-domain variational measurement, in which the homodyne detection phase varies in time. This protocol allows us to characterize the macroscopic quantum state below the Heisenberg Uncertainty – i.e. *Quantum Tomography* – and the only limitation comes from readout loss which enters in a similar manner as the frequency-domain variational scheme proposed by Kimble *et al.* [1]. In the case of no readout loss, it is identical to the back-action-evading scheme invented by Vyatchanin *et al.* [2] for detecting gravitational-wave (GW) signal with known arrival time. As a special example and to motivate *Macroscopic Quantum Mechanics* (MQM) experiments with future GW detectors, we mostly focus on the *free-mass limit* – the characteristic measurement frequency is much higher than the oscillator frequency – and further assume the classical noises are Markovian, which captures the main feature of a broadband GW detector. Besides, we consider verifications of Einstein-Podolsky-Rosen (EPR) type entanglements between macroscopic test masses in GW detectors, which enables to test one particular version of *Gravity Decoherence* conjectured by Diósi and Penrose [3, 4].

I. INTRODUCTION

Due to recent advancements in fabricating lossless devices, various types of macroscopic systems can soon approach the quantum regime [5–11], which will be able to test the quantum mechanics of macroscopic objects. The common strategy of those experiments is preparing a macroscopic quantum state of the mechanical oscillator through continuous position measurements. Quantum mechanically, if the oscillator position is being continuously monitored, a certain classical trajectory in phase-space can be mapped out and the oscillator is projected into an *a posteriori state* [12] which is also called conditional quantum state [6, 13–17].

In Ref. [17], we provided in great details a survey of the first principles for preparation of macroscopic Gaussian quantum state and creation of entanglements between two macroscopic objects. The general analysis of this work is independent of the object's scale and mass – these parameters will only modify the structure of the arising noise – as long as the object is in a Gaussian state of the center of mass position and momentum. In particular, we applied our formalism to discuss the MQM experiments with macroscopic test masses in GW detectors. We demonstrated explicitly that given the design classical-noise budget, next-generation GW detectors such as Advanced LIGO [18] and Cryogenic Laser Interferometer Observatory (CLIO) [19] can prepare a nearly Heisenberg-Limited Gaussian quantum state and create EPR-type quantum entanglements between macroscopic test masses. Besides, we showed that, the free-mass *Standard Quantum Limit* (SQL) [20–22] for the sensitivity of detecting GW, as given by

$$S_x^{\rm SQL}(\Omega) = \frac{2\hbar}{m\,\Omega^2}\,, \tag{1}$$

also serves as a benchmark for the MQM experiments with GW detectors. More concretely, we related the purity of the conditional quantum state of test masses to the SQL-beating ratio of the classical noise, and the degree of achievable entanglement to the size of the frequency window (ratio between upper and lower ends of that frequency window) in which the classical noise budget goes below the SQL.

However, it is impossible to verify the prepared conditional state from the output data used for the conditioning process. This is because the output in the state-preparation process only allows to measure the classical trajectory of the object – quantum fluctuations are only inferred from classical-noise budget, but not directly visible. Therefore, it calls for a second measurement stage which has to follow up the preparation stage. In this paper, we will address the above issue by considering a subsequent *state verification* procedure, in which we probe the conditional state obtained during the preparation stage ($t < 0$) with an accuracy superior than the Heisenberg Uncertainty. Indeed, to probe a quantum state, e.g. its Wigner function, we need to synthesize the marginal distribution of different quadratures $\hat{X}_\zeta$, and

$$\hat{X}_\zeta \equiv \hat{x}(0)\cos\zeta + \frac{\hat{p}(0)}{m\,\omega_m}\sin\zeta. \tag{2}$$

Since for a single measurement setup, different quadratures do not commute with each other, namely

$$[\hat{X}_\zeta,\,\hat{X}_{\zeta'}] = \frac{i\,\hbar}{m\,\omega_m}\sin(\zeta-\zeta'), \tag{3}$$

one needs multiple setups and each measures at a particular quadrature $\hat{X}_\zeta$ with an accuracy below the Heisenberg limit – the synthesis of these measurements yields a quantum tomography. As we will show, for each quadrature, a sub-Heisenberg accuracy can be achieved by adopting an optimal time-domain variational scheme, in which the homodyne detection phase is time-dependent. If there is no loss in the readout, the measurement-induced back action can be completely evaded, which recovers the scheme first invented by Vyatchanin *et al.* [2] for detecting gravitational waves with known arrival time. Beside, we also assume that squeezed vacuum can be injected right at the beginning of the verification process. As in Ref. [17], we will demonstrate that in the free-mass limit, the SQL (cf. Eq. (1)) again sets the benchmark for the success of sub-Heisenberg tomography.

Additionally, verification of quantum state below the Heisenberg Limit naturally allows us to test whether macroscopic entanglements can indeed be established, as predicted in Ref. [16, 17], and how long such entangled state can survive. In fact, survival of macroscopic entanglement can be used to test a particular version of gravity decoherence conjectured by Diósi [3] and Penrose [4]. Although for an individual object it is not entirely clear the classical superposition of what *pointer* states gravity decoherence will drive it into. While for an entangled state among multiple objects, even though Gaussian, it would naturally have to decay into the one that is not entangled, within the gravity decoherence time scale.

In this paper, we will constrain ourselves to MQM experiments with Markovian noise. Specifically, we will consider broadband interferometers with arm-cavity bandwidth far broader than their measurement frequency scale, and situations where the spectra of the classical sensing noise (such as the mirror internal thermal noise) and of the classical force noise (such as the suspension thermal noise) can be modeled as white noises. Non-Markovianity of noise sources – although they certainly arise in actual GW detectors [17] and will be crucial for the success of a real experiment – is a rather technical issue. The non-Markovianity will not change the results presented here significantly, as we will show and address in a separate paper [23].

This paper is organized as follows: in Sec. II, we provide the timeline of a full MQM experiment with preparation and verification, and use simple order-of-magnitude estimates to convince ourselves that our proposal is indeed plausible; in Sec. III, we calculate state verification accuracy in presence of Markovian noise (largely confirming the order-of-magnitude estimates, but with precise numerical factors); in Sec. IV, we apply this scheme to verify the macroscopic quantum entanglements between test masses in GW detectors as a test of gravity decoherece; in Sec. V, we summarize our main results. In the Appendix, we present technical details for obtaining the optimal variational scheme during the verification.

II. OUTLINE OF EXPERIMENT WITH ORDER-OF-MAGNITUDE ESTIMATE

A. Approximate noise budget

We will simplify the arising noise in a typical MQM experiment by assuming that both the quantum and the classical noises are purely Markovian. A more detailed discussion on quantum and classical noise is presented in Sec. III A of Ref. [17]. In the free-mass limit, the displacement sensitivity of the device is given by the position-referred noise spectrum [1],

$$S_x = \underbrace{\frac{\hbar}{m\,\Omega^2}\left[\frac{\Omega^2}{\Omega_q^2}+\frac{\Omega_q^2}{\Omega^2}\right]}_{S_{\rm quant}} + \underbrace{\frac{2\hbar}{m\,\Omega^2}\frac{\Omega_F^2}{\Omega^2}}_{S_{\rm force}} + \underbrace{\frac{2\hbar}{m\,\Omega_x^2}}_{S_{\rm sens}}\,, \tag{4}$$

with the characteristic frequencies for the measurement given by Ω_q and for the classical thermal and sensing noises by Ω_F and Ω_x respectively. In this equation, we have summarized white shot and classical sensing noises as

$$S_x^q = \frac{\hbar}{m\,\Omega_q^2}\,, \quad S_x^{\rm th} = \frac{2\,\hbar}{m\,\Omega_x^2} \equiv 2\,\zeta_x^2\,S_x^q \tag{5}$$

and white back-action and classical force noises given by

$$S_F^q = \hbar\,m\,\Omega_q^2\,, \quad S_F^{\rm th} = 2\,\hbar\,m\,\Omega_F^2 \equiv 2\,\zeta_F^2\,S_F^q\,. \tag{6}$$

The classical sensing noise is defined as the difference between the object's center of mass motion and its surface motion which is actually being measured. We shall further denote two characteristic time scales by

$$\tau_q \equiv 1/\Omega_q\,, \quad \tau_F \equiv 1/\Omega_F\,. \tag{7}$$

Note that Ω_q, Ω_F, and Ω_x are the frequencies at which the quantum noise, force noise and classical sensing noise intersect the SQL (cf. Eq. (1)), respectively, and that we have defined $\zeta_F = \Omega_F/\Omega_q$ and $\zeta_x = \Omega_q/\Omega_x$.

B. Timeline of proposed experiment

Before providing an order-of-magnitude estimate of the preparation and verification processes, we will first de-

[1] Here and throughout the paper we make use of *single-sided* definition of spectral density of arbitrary observable $\hat{o}$ that is defined according to Wiener-Khinchin theorem as:

$$S_{o_1 o_2}(\Omega) = 2\int_0^\infty d\tau e^{i\omega\tau}\langle\hat{o}_1(0)\hat{o}_2(\tau)\rangle_{\rm sym}\,,$$

where angular brackets $\langle\,\rangle_{\rm sym}$ stand for *symmetrized* ensemble average, *i.e.* for system in quantum state characterized by density matrix $\hat{\rho}$, it is defined as

$$\langle\hat{o}_1(0)\hat{o}_2(\tau)\rangle_{\rm sym} \equiv {\rm Tr}\left[\frac{1}{2}(\hat{o}_1(0)\hat{o}_2(\tau)+\hat{o}_2(\tau)\hat{o}_1(0))\hat{\rho}\right]\,.$$

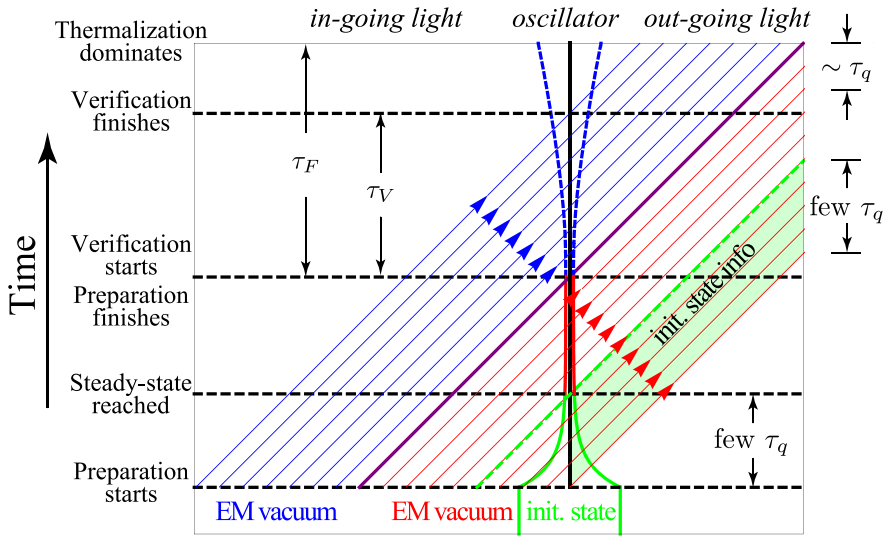

FIG. 1: Space-time diagram showing the timeline of our proposed MQM experiment (see Sec. II B for detailed explanations). Left part of the plot represents the region of in-going light. The mechanical oscillator world line is shown as vertical line in the middle. The right part of the plot represents the region of out-going light (even though in reality light may escape from the same side as they enter). We show light rays in preparation and verification stages in red and blue, with a purple ray separating the two sets. Conditional variance of test-mass motion is represented in solid curves alongside the central vertical line (not drawn to the same scale as light propagation). At the beginning of preparation, it is dominated by that of the initial state (green), after a transient, it is dominated by incoming radiation and detection quadrature (thus shown in red); during state verification, we show the expected growth of test-mass variance due to classical noise alone, but ignoring the effect of radiation-pressure fluctuations, because we use back-action evasion (show in blue).

scribe in details the timeline of a plausible MQM experiment in an interferometric setup. We have sketched a space-time diagram of this experiment in Fig. 1 — with time going upward, therefore we start from the bottom of the figure.

Lock Acquisition. At the beginning, the mechanical oscillator is in a highly classical state[2], so is the optical field. Therefore, the first step is to "acquire lock" of the interferometer, and reach a steady-state operation mode, during which several τ_q (measurement scale) will have elapsed. From this time and on, the initial state of the oscillator will have been forgotten (propagating outward within the green strip in Fig. 1), and the state of the system will be determined by the driving fields, including classical force and sensing noises, as well as quantum noise. This will be the beginning of our state-preparation stage (region above the 45° green dashed line in Fig. 1).

State Preparation. This stage is the same as a steady-state operation of the interferometer. The quantum state of the oscillator is collapsed continuously due to homodyne readouts of the photocurrent. At any instant t during state preparation, based on the measured history of the photocurrent (mostly on data within several times τ_q to the past of t), *conditional expectation* of the mirror position $\hat{x}^{\rm cond}$ and momentum $\hat{p}^{\rm cond}$ can be constructed, and $(\hat{x}^{\rm cond}, \hat{p}^{\rm cond})$ will be randomly walking in the phase space. Quantum mechanically, they are the center of the oscillator's instantaneous Wigner function, which we assume to be Gaussian. The secondary moments, describable by the *covariance matrix* (CM) between position and momentum, which consists of $V_{xx}^{\rm cond}$, $V_{xp}^{\rm cond}$ and $V_{pp}^{\rm cond}$, can be calculated from the noise budget of the interferometer — they, together with $\hat{x}^{\rm cond}$ and $\hat{p}^{\rm cond}$, fully describe the quantum state of the oscillator at any instant. In our situation of Gaussian steady state, the construction of $(\hat{x}^{\rm cond}, \hat{p}^{\rm cond})$ from the history of the photocurrent can be accomplished most easily using Wiener Filtering, as shown in Ref. [17]. We will decide to terminate the preparation stage at $t = 0$, when $(\hat{x}^{\rm cond}, \hat{p}^{\rm cond})$ will be determined by data from several $-\tau_q$ up to 0 (as shown by the yellow stripe in Fig. 1).

State Verification. Although the instantaneous conditional state of the mirror at $t = 0$ is calculable from the photocurrents and the noise budget, a direct tomography measurement of its Wigner function provides a verification of the calculation which not only depends on our understanding of the calibration of classical-noise budget, but also on the correctness of quantum mechanics – for example, we do want to directly verify the macroscopic EPR-type entanglement between mirrors that we predicted to exist [16, 17]. In addition, if we insert an *evolution stage* after state preparation, in which the system evolves in time, the verification stage can also serve

[2] By "classical", we mean highly impure quantum state, i.e. its occupation number is much larger than unity.

as a check of whether the evolution happens as predicted by quantum mechanics. Moreover, if we were able to prepare non-Gaussian states with non-positive-definite Wigner function during the evolution stage, as suggested by Khalili recently [24], and then verification is crucial in exposing the negative region of the Wigner function. In Fig. 1, a purple 45° line is drawn between preparation and verification stages, and blue lines are used to represent light interacting with the oscillator in the verification stage — symbolizing the fact that in principle, a different observer could perform the verification process, and verify the quantum state by him/herself. The only knowledge from the preparer would be the conditional expectation $x^{\rm cond}$ and $p^{\rm cond}$. This is indeed true if all noise sources are Markovian. While the noise spectra are colored, the verification process will need more *classical information* obtained during the preparation stage, in order to make a sub-Heisenberg tomography of the quantum state of the test mass, as we will discuss in a later paper [23].

In order to measure a particular quadrature with a sub-Heisenberg accuracy, we will employ a local oscillator light whose phase is time-dependent, and optimize this phase, as well as the weight with which data collected at different time would be combined (cf. Sec. III). As it turns out, in the case when there is no readout loss, this optimization automatically gives a detection scheme that evades measurement back action, the same as the one proposed by Vyatchanin [2] for the detection of gravitational-wave signals with known arrival time. Since gravitational-wave signals with known arrival time are usually not anticipated, such time-domain variational schemes will not be as useful for gravitational-wave detection as the frequency-domain variational scheme invented later by Kimble *et al.* [1].

The verification lasts for a time scale between the measurement time scale τ_q and the thermal decoherence scale τ_F, after which the diffusion of $\hat{x}$ and $\hat{p}$ in the phase space becomes much larger than their vacuum level. This process is shown in Fig. 1, and explained qualitatively in Sec. II D.

C. Preparation stage

The mathematical treatment of state preparation has been given in Ref. [17]. To motivate MQM experiments with macroscopic test masses in next-generation GW detectors, we focused on the regime where the characteristic measurement frequency Ω_q is much higher than the test-mass frequency ω_m (free-mass-limit), such that the test-mass can be well approximated as a free mass. By measuring the output phase quadrature, we showed that the *conditional variances* of test-mass location and momentum ($\hat{x}$ and $\hat{p}$) are given by following CM (cf. Eq. (52)–(54) of Ref. [17])

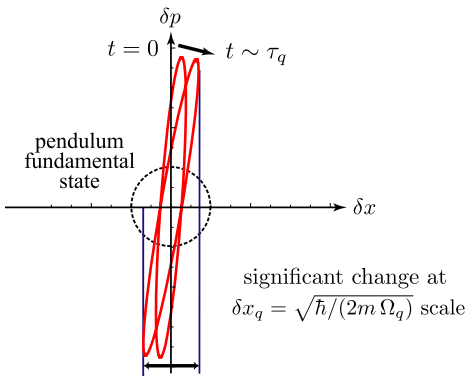

FIG. 2: Highly position-squeezed conditional state and minimum time scale required for state verification.

$$\mathbf{V}^{\rm cond} = \begin{bmatrix} N_F^{\frac{1}{4}} N_x^{\frac{3}{4}} \sqrt{2}\delta x_q^2 & N_F^{\frac{1}{2}} N_x^{\frac{1}{2}} \hbar/2 \\ N_F^{\frac{1}{2}} N_x^{\frac{1}{2}} \hbar/2 & N_F^{\frac{3}{4}} N_x^{\frac{1}{4}} \sqrt{2}\delta p_q^2 \end{bmatrix} \tag{8}$$

where we have denoted

$$N_x \equiv 1 + 2\zeta_x^2\,, \quad N_F \equiv 1 + 2\zeta_F^2 \tag{9}$$

while

$$\delta x_q^2 \equiv \hbar/(2m\,\Omega_q)\,, \quad \delta p_q^2 \equiv \hbar\, m\,\Omega_q/2 \tag{10}$$

are zero-point uncertainties in position $\hat{x}$ and momentum $\hat{p}$ of an Ω_q harmonic oscillator. Note that these variances would be consistent with a Heisenberg-Limited state, if classical noises are absent (instead of *twice* Heisenberg Limit, as could be naively expected since the test-mass is "being measured": measurement imposes the Heisenberg Uncertainty, instead of adding on to it).

The above conditional variances can also be obtained from an order-of-magnitude estimate. Given a measurement time scale of τ, we would have

$$\delta x^2 \sim S_x^{\rm tot}/\tau + \tau^3 S_F^{\rm tot}/m^2 \sim N_x^{\frac{3}{4}} N_F^{\frac{1}{4}} \delta x_q^2 \tag{11}$$

$$\delta p^2 \sim m^2 S_x^{\rm tot}/\tau^3 + \tau S_F^{\rm tot} \sim N_x^{\frac{1}{4}} N_F^{\frac{3}{4}} \delta p_q^2 \tag{12}$$

where $S_x^{\rm tot} \equiv S_x^q + S_x^{\rm th}$, $S_F^{\rm tot} \equiv S_F^q + S_F^{\rm th}$, with optimal measurement time given by $\tau \sim \tau_q$.

D. Verification stage

To verify the prepared conditional quantum state, we first realize that we only obtain information about $\hat{x}(0)$ and $\hat{p}(0)$ by measuring location, but at different time. In order for an entire state characterization to be possible, one might then expect that an oscillation period must pass and during this time, the thermal noise causes an

insignificant diffusion of the oscillator momentum compared with its zero-point uncertainty, which requires [22]

$$\frac{k_B T}{\hbar\,\omega_m} < Q_m \tag{13}$$

with T denoting the environmental temperature and Q_m the mechanical quality factor. This requirement is unnecessary if the initial quantum state is prepared by a strong measurement as in the case of using next-generation GW detector ($\Omega_q \gg \omega_m$). This is because the conditional quantum state is *highly squeezed in location*, and it only takes $t \sim \tau_q$ for initial momentum fluctuation to enter and begin to dominate fluctuations in the oscillator position as shown in Fig. 2. This means, depending on the particular strategy, one can extract $\hat{x}$ and $\hat{p}$ *below the levels of* δx_q, and δp_q, respectively, if one is able to measure oscillator position with an accuracy better than δx_q, within a time scale of several τ_q. This is certainly possible; in fact, we can give a more detailed order-of-magnitude estimate. With the back-action-evading (BAE) scheme, we have

$$\delta x_V^2 \sim S_x^{\rm tot}/\tau + \tau^3 S_F^{\rm th}/m^2 \ \sim N_x^{3/4}\zeta_F^{1/2}\delta x_q^2 \tag{14}$$

$$\delta p_V^2 \sim m^2 S_x^{\rm tot}/\tau^3 + \tau S_F^{\rm th} \sim N_x^{1/4}\zeta_F^{3/2}\delta p_q^2\,, \tag{15}$$

with

$$\delta x_V \delta p_V \sim N_x^{1/2}\zeta_F \hbar/2 \tag{16}$$

Here the optimal verification time would be $\tau_V \sim \zeta_F^{-1/2}\tau_q$ and $\tau_q < \tau_V < \tau_F$. (This is reflected in the left panel of Fig. 1.) Note that this error can be arbitrarily small by lowering ζ_F indefinitely, i.e. a strong measurement, while a sub-Heisenberg accuracy can be achieved when $\zeta_F < 1$. If we inject phase squeezing during the verification stage, we would have

$$\delta x_V \delta p_V \sim (e^{-2q} + 2\zeta_x^2)^{1/2}\zeta_F\hbar \tag{17}$$

Increasing squeezing factor always improves our verification sensitivity, with a limit of

$$(\delta x_V \delta p_V)_{\rm lim}^{\rm BAE} \sim \zeta_x\zeta_F\hbar. \tag{18}$$

Had we not evaded the back-action noise, we would have $\sqrt{N_F}$ in the place of ζ_F, which means $\delta x_V \delta p_V$ would be Heisenberg-Limited — unless different squeezing factors are assumed. For low squeezing (i.e., $e^{\pm q}$ both bigger than ζ_x and ζ_F), we need phase squeezing for $\hat{x}$ observation, amplitude squeezing for $\hat{p}$ observation, with

$$\delta x_V \delta p_V \sim e^{-q}\hbar\,, \tag{19}$$

which is a significant factor $(1/\zeta_F)$ worse than the BAE scheme. Even though there exists an optimal squeezing factor that this scheme can apply and yields

$$(\delta x_V \delta p_V)_{\rm opt}^{\rm conv} \sim \zeta_x\hbar\,, \tag{20}$$

yet it is still worse than the limiting situation of the BAE scheme by a factor of $1/\zeta_F$.

III. STATE VERIFICATION IN THE PRESENCE OF MARKOVIAN NOISE

In this section, we will treat the state verification with Markovian noise in details. This can justify the order-of-magnitude estimate we have done in previous section. Besides, we will show explicitly how to construct the optimal variational scheme that gives a sub-Heisenberg accuracy.

A. Equations of motion and dynamics of the conditional quantum state

In this subsection, we will analyze the dynamics of the conditional quantum state and evolution of the conditional variance. This shows the necessity of back-action evading during the verification process, which will be addressed thoroughly in the next subsection.

The equations of motion (EOM) for the center of mass of the oscillator, which are valid for $t > 0$, can be written as

$$\hat{p}(t) = m\,\dot{\hat{x}}(t), \tag{21}$$

$$\dot{\hat{p}}(t) + \gamma_m\hat{p}(t) + m\,\omega_m^2\hat{x}(t) = \alpha\,\hat{a}_1(t) + \hat{\xi}_F(t), \tag{22}$$

where ω_m is the mechanical frequency; γ_m is the damping rate and $\alpha \equiv (\hbar\, m\,\Omega_q^2)^{1/2} = (8\,P\,\omega_0\,\hbar/c^2)^{1/2}$ is the coupling constant between the oscillator and light with P denoting the intra-cavity optical power. The above equations describe the oscillator motion driven by back action $\alpha\,\hat{a}_1$ as well as by classical Markovian thermal force $\hat{\xi}_F$, which has the correlation

$$\langle\hat{\xi}_F(t)\,\hat{\xi}_F(t')\rangle_{\rm sym} = S_F^{\rm th}\ \delta(t-t')/2\,. \tag{23}$$

The amplitude quadrature operator $\hat{a}_1$ of the in-going vacuum fields obeys the correlation

$$\langle\hat{a}_1(t)\ \hat{a}_1(t')\rangle_{\rm sym} = \ e^{2\,q}\,\delta(t-t')/2\,, \tag{24}$$

with q denoting the squeezing factor. In the paraxial and narrow-band approximation, the amplitude and phase quadratures $\hat{a}_{1,2}$ are related to the electric field with central frequency ω_0 by $\hat{E}(t) \equiv \hat{E}_1(t)\,\cos\omega_0 t + \hat{E}_2(t)\,\sin\omega_0 t$, where $\hat{E}_i(t) = (4\pi\hbar\,\omega_0/\mathcal{S}\,c)^{1/2}\,\hat{a}_i(t)$ $(i = 1, 2)$ with $\mathcal{S}$ standing for the effective cross section area of the laser beam [1, 25].

In the following, we will consider an oscillator with a high quality factor, i.e. $\omega_m \gg \gamma_m$. Within a time scale much shorter than $1/\gamma_m$, the oscillator can be well approximated as a free oscillator. Corresponding, the analytical solution to the oscillator position in Eq. (21) can be written as

$$\hat{x}(t) = \hat{x}_q(t) + \int_0^\infty {\rm d}t'\,G_x(t-t')\,[\alpha\,\hat{a}_1(t') + \xi_F(t')]\,. \tag{25}$$

Here we have defined the Green's function as

$$G_x(t) = \Theta(t)\,\frac{\sin(\omega_m\,t)}{m\,\omega_m}\,, \tag{26}$$

with $\Theta(t)$ denoting the Heaviside function; $\hat{x}_q$ represents the free quantum oscillation of the oscillator, which is given by

$$\hat{x}_q(t) = \delta x_q \left[\hat{X}_0\, f_1(t) + \hat{P}_0\, f_2(t)\right], \tag{27}$$

where we have defined

$$f_1(t) \equiv \cos\omega_m t\,, \quad f_2(t) \equiv \frac{\Omega_q \sin\omega_m t}{\omega_m}, \tag{28}$$

and

$$\hat{X}_0 \equiv \hat{x}^{\rm cond}(0)/\delta x_q\,, \quad \hat{P}_0 \equiv \hat{p}^{\rm cond}(0)/\delta p_q\,. \tag{29}$$

Note that the quantum oscillation $\hat{x}_q(t)$ actually corresponds to the signal that we seek to probe in the verification process.

Due to the back action and thermal decoherence, the variances of the conditional quantum state will start to grow at $t > 0$. Explicitly, the covariance matrix evolves as

$$\mathbf{V}(\tau) = \mathbf{R}_\Phi^T\, \mathbf{V}^{\rm cond}\, \mathbf{R}_\Phi + \frac{S_F^{\rm tot}}{8\,m^2\omega_m^3} \begin{bmatrix} 2\,\Phi - \sin 2\,\Phi & 2\,m\,\omega_m \sin^2\Phi \\ 2\,m\omega_m \sin^2\,\Phi & m^2\omega_m^2\,(2\,\Phi + \sin 2\,\Phi) \end{bmatrix}, \tag{30}$$

where $\Phi \equiv \omega_m\,\tau$, $S_F^{\rm tot} = S_F^q + S_F^{\rm th}$ and the rotating matrix $\mathbf{R}_\Phi$ is given by

$$\mathbf{R}_\Phi = \begin{bmatrix} \cos\Phi & -m\,\omega_m \sin\Phi \\ (m\,\omega_m)^{-1}\sin\Phi & \cos\Phi \end{bmatrix}. \tag{31}$$

The first term in $\mathbf{V}(\tau)$ simply represents the rotation of the CM, while the second term is contributed by the back-action and thermal noises, which will induce diffusion of $\hat{x}$ and $\hat{p}$ in the phase space.

In the free-mass limit with $\Omega_q \gg \omega_m$, for $\tau \ll 1/\omega_m$, the above formulas for the CM can be expanded as series of Φ ($\Phi \ll 1$). Up to the leading order of Φ, we have

$$V_{xx}(\theta) = V_{xx}^{\rm cond} + \frac{4\delta x_q^2}{\hbar} V_{xp}^{\rm cond}\,\theta + \frac{\delta x_q^2}{\delta p_q^2} V_{pp}^{\rm cond}\,\theta^2 + \delta x_q^2\left(e^{2\,q} + 2\,\zeta_F^2\right)\frac{\theta^3}{3}\,, \tag{32}$$

$$V_{xp}(\theta) = V_{xp}^{\rm cond} + \frac{\hbar}{2\delta p_q^2} V_{pp}^{\rm cond}\,\theta + \frac{\hbar}{4}(e^{2\,q} + 2\,\zeta_F^2)\theta^2\,, \tag{33}$$

$$V_{pp}(\theta) = V_{pp}^{\rm cond} + \delta p_q^2 (e^{2\,q} + 2\,\zeta_F^2)\,\theta \tag{34}$$

with $\theta \equiv \Omega_q\tau$ and $V_{xx,xp,pp}^{\rm cond}$ denoting the elements of $\mathbf{V}^{\rm cond}$. Due to the free evolution, Eqs. (32)–(33) indicate that there is a mixing in the conditional variances. When $\theta \gtrsim 1$, or equivalently $\tau \gtrsim \tau_q$, the initial momentum fluctuation $V_{pp}^{\rm cond}$ becomes the dominant fluctuations in $\hat{x}$ due to the fact that we have highly position-squeezed state, as we have mentioned previously. Besides, the additional growth of variance due to force noises is actually the problems one has to face during the verification process and it sets forth an optimal time scale for the verification.

The growth becomes more clear by defining the purity U of quantum state as in Ref. [17], up to the first order of θ,

$$U(\theta) \equiv \frac{2}{\hbar}\sqrt{\det\mathbf{V}(\theta)} \approx U(0) + \frac{1}{2\delta x_q^2}(e^{2q} + 2\zeta_F^2) V_{xx}^{\rm cond}\theta + \mathcal{O}(\theta^2), \tag{35}$$

with $U(0) \equiv \sqrt{\det\mathbf{V}^{\rm cond}}$. Since the probing light is phase squeezed with $e^{2q} \gg 1$ in the verification process, this indicates that the quantum back action creates much stronger decoherence than the thermal noise ($\zeta_F \ll 1$), i.e. causing a faster growth in the purity. In order to achieve sub-Heisenberg accuracy, back-action-evading is essential in the verification stage, as will be investigated in great details in the next subsection.

B. Time-dependent homodyne detection and back-action evasion

At $t > 0$, we turn on the verification process, and the corresponding Heisenberg EOM for the optical fields, which are actually valid for both preparation $t < 0$ and verification $t > 0$, can be written as

$$\hat{b}_1(t) = \hat{a}_1(t) + \sqrt{\eta}\,\hat{n}_1(t), \tag{36}$$

$$\hat{b}_2(t) = \hat{a}_2(t) + \sqrt{\eta}\,\hat{n}_2(t) + \frac{\alpha}{\hbar}\,[\hat{x}(t) + \hat{\xi}_x(t)]. \tag{37}$$

Here $\hat{b}_i$ are the output quadratures; the vacuum field quadratures $\hat{n}_{1,2}$ originate from non-unity quantum efficiency of the photodetector; $\hat{\xi}_x$ corresponds to the classical sensing noise. We note that among the out-going fields, $\hat{b}_1$ is pure noise, while $\hat{b}_2$ contains both signal and noise. In order to highlight this, we write

$$\hat{b}_1(t) = \delta\hat{b}_1(t)\,, \tag{38}$$

$$\hat{b}_2(t) = \delta\hat{b}_2(t) + \frac{\alpha}{\hbar}\,\hat{x}_q(t) \tag{39}$$

with (cf. Eq. (25))

$$\delta\hat{b}_2(t) = \hat{a}_2(t) + \sqrt{\eta}\,\hat{n}_2(t) + \frac{\alpha}{\hbar}\,\xi_x(t) + \frac{\alpha}{h}\int_0^\infty {\rm d}t'\, G_x(t-t')\,\left[\alpha\,\hat{a}_1(t') + \hat{\xi}_F(t')\right]. \tag{40}$$

In this way, we can directly see that measuring an appropriate combination of the two output quadratures can allow to remove the back-action noise that is imposed onto the oscillator during the verification process at $t > 0$. Searching for such an optimal combination is the main issue to be addressed in this section.

In order to study the instantaneous distribution of an arbitrary oscillator quadrature $\hat{X}_\zeta$ at $t = 0$, we apply homodyne detection of the outgoing optical field

$$\hat{B}_{\rm out}(t) = \hat{b}_1 \cos\omega_0 t + \hat{b}_2 \sin\omega_0 t \tag{41}$$

at $t > 0$ by mixing it with strong local oscillator light $L(t)$ with time-dependent amplitude and phase, namely

$$L(t) = L_1(t)\cos\omega_0 t + L_2(t)\sin\omega_0 t \tag{42}$$

with L_1 and L_2 corresponding to the amplitude and phase modulation respectively. Through a low-pass filtering (with bandwidth much smaller than ω_0) of the beating signal, the resulting photocurrent is given by

$$\hat{i}(t) \propto 2\overline{\hat{B}_{\rm out}(t)L(t)} = L_1(t)\hat{b}_1(t) + L_2(t)\hat{b}_2(t)\,, \tag{43}$$

where overline means averaging over many optical oscillation periods. Note that Heisenberg operator of the photocurrent commutes at different time, i.e.

$$[\hat{i}(t), \hat{i}(t')] = 0\,, \tag{44}$$

and are therefore *simultaneously measurable*, as obviously expected. Based on measurement result of $\hat{i}(t)$ from 0 to $T_{\rm int}$, we can apply a digital filtering and construct a weighted quantity $\hat{Y}$, which is given by

$$\hat{Y} = \int_0^{T_{\rm int}} W(t)\hat{i}(t)dt \equiv (g_1|\hat{b}_1) + (g_2|\hat{b}_2)\,, \tag{45}$$

where $W(t)$ denoting the weighting function and $g_{1,2}(t) \equiv W(t)\,L_{1,2}(t)$, and

$$(A|B) \equiv \int_0^{T_{\rm int}} A(t)B(t)dt\,. \tag{46}$$

Note that the overall re-scaling of $g_{1,2}(t) \to Cg_{1,2}(t)$ with C an time-independent constant does not affect our verification performance, and that there are multiple ways of achieving a particular set of $g_{1,2}(t)$, by adjusting the amplitude/phase modulation of the local oscillator and the weighting function $W(t)$.

In light of Eqs. (25), (38)–(40) and (45), we decompose the weighted quantity

$$\hat{Y} = \hat{Y}_s + \delta\hat{Y} \tag{47}$$

as a signal $\hat{Y}_s$ and a noise part $\delta\hat{Y}$. They are given by

$$\begin{aligned} \hat{Y}_s &= \frac{\alpha}{\hbar}\left[(g_2|f_1)\hat{X}_0 + (g_2|f_2)\hat{P}_0\right]\delta x_q, \\ \delta\hat{Y} &= (g_1|\delta\hat{b}_1) + (g_2|\delta\hat{b}_2). \end{aligned} \tag{48}$$

Since the overall normalization of $g_{1,2}$ does not matter, if we want to detect the oscillator position at a quadrature ζ, we can simply impose, mathematically, that

$$(g_2|f_1) = \cos\zeta\,, \quad (g_2|f_2) = \sin\zeta\,. \tag{49}$$

For the noise part, we have

$$\begin{aligned} \delta\hat{Y} &= (g_1|\hat{a}_1 + \sqrt{\eta}\,\hat{n}_1) + (g_2|\hat{a}_2 + \sqrt{\eta}\,\hat{n}_2) \\ &+ \frac{\alpha^2}{\hbar}(g_2|\mathbf{G}_x|\hat{a}_1) \\ &+ \frac{\alpha}{\hbar}\left[(g_2|\mathbf{G}_x|\xi_F) + (g_2|\xi_x)\right]\,, \end{aligned} \tag{50}$$

where integration with $G_x(t-t')$ has been augmented into applying the linear operator $\mathbf{G}_x$ on $\mathcal{C}^\infty[0, T_{\rm int}]$ space. In the above equation, terms on the first line is the shot noise and the term on the second line is the back-action noise, while terms on the third line are the classical force and sensing noises.

From Eq. (49), we can see that all possible quadratures can be probed by choosing different digital weighting function $W(t)$. Besides, given one particular setup with fixed amplitude modulation $L_1(t)$ and phase modulation $L_2(t)$ of the local oscillator, the additional noise can still be further minimized by applying an optimal $W(t)$. One might then naively expect that a quantum tomography can be achieved simply with optimal digital filtering. However, this is prohibited by quantum mechanics. As also mentioned in the introduction, on the one hand, for a single measurement setup, different quadratures do not commute, i.e. the signal part of the readouts

$$[\hat{Y}_s(\zeta), \hat{Y}_s(\zeta')] = 2i\frac{\alpha^2}{\hbar^2}\delta x_q^2 \sin(\zeta - \zeta'), \tag{51}$$

while, on the other hand, $[\hat{Y}(\zeta), \hat{Y}(\zeta')] = 0$ as a consequence of Eq. (44). It immediately follows that

$$[\delta\hat{Y}(\zeta), \delta\hat{Y}(\zeta')] = -2i\frac{\alpha^2}{\hbar^2}\delta x_q^2 \sin(\zeta - \zeta'). \tag{52}$$

This means that the additional noise $\delta\hat{Y}$ must be Heisenberg limited, as was also shown previously by Buonanno *et al.* [26] in discussing the quantum noise of the optimal heterodyne readout scheme for detecting gravitational-waves. Therefore, to obtain an sub-Heisenberg tomography, we need to design separate optimal measurement schemes for each quadrature by choosing different $L_1(t)$ and $L_2(t)$ rather than only varying $W(t)$. Mathematically, this means that the additional verification noise is a functional that has two independent degrees of freedom $g_1(t)$ and $g_2(t)$ instead of one degree of freedom $W(t)$.

The optimal $g_1(t)$ and $g_2(t)$ that give an sub-Heisenberg accuracy for each quadrature will be rigorously derived for the general cases in the next section. If $\hat{a}_1$ and $\hat{a}_2$ are uncorrelated and there is *no optical loss* with $\eta = 0$, we can immediately see that an *optimal choice* for g_1 would be to cancel the entire contribution from the back-action term $\hat{a}_1$. This is equivalent to impose that

$$(g_1|\hat{a}_1) + \frac{\alpha^2}{h}(g_2|\mathbf{G}_x|\hat{a}_1) = 0 \tag{53}$$

or

$$|g_1) + \frac{\alpha^2}{\hbar}\mathbf{G}_x^{\rm adj}|g_2) = 0\,, \tag{54}$$

where $\mathbf{G}_x^{\rm adj}$ is the adjoint of $\mathbf{G}_x$. Physically, this corresponds to bringing in a piece of shot noise, $(g_1|\hat{a}_1)$ to cancel the back-action noise, $\alpha^2/h(g_2|\mathbf{G}_x|\hat{a}_1)$ — therefore achieving a only shot-noise-limited measurement. Writing out Eq. (54) more explicitly, this is

$$g_1(t) + (\alpha^2/\hbar)\int_t^{T_{\rm int}} dt' G_x(t'-t)g_2(t') = 0, \tag{55}$$

which agrees exactly with the "variational-type" BAE measurement scheme first investigated by Vyatchanin *et al.* [2]. It is suitable for detecting signals with *known arrival time*. For stationary GW signals, one would prefer frequency-domain variational techniques proposed by Kimble *et al.* [1], which evades back-action noise also for all possible signals as long as they are Gaussian and stationary processes.

As realized by Kimble *et al.* [1] in their frequency-domain treatment, when optical loss is significant (large η) and/or when back-action noise is strong (large α), variational approach becomes less effective, because in such a case, the magnitude of g_1 required to bring enough $\hat{a}_1$ to cancels with back-action noise would also introduce significant noise $\hat{n}_1$ due to optical losses. This reasoning apparently leads to the need of a trade-off between the need to evade back action and the need to minimize loss-induced shot noise — such an optimization will be made in the next section.

C. Optimal verification scheme and additional noise covariance: formal derivation

Imposing BAE does not specify the shape of g_2, nor do Eqs. (49), and we have further freedom in choosing a g_2 that minimizes noise in measuring a particular quadrature of $\hat{X}_\zeta$. In addition, in presence of optical losses, totally evading back action is not the obvious optimum, and therefore we need to optimize g_1 and g_2 simultaneously. In this section, we first carry out this procedure formally, and apply to the Markovian-noise budget in the next subsection.

Subject to the constraints in Eq. (49), the total normalized noise variance σ^2 for measuring $\hat{X}_\zeta$ can be written as a functional of $g_{1,2}$,

$$\sigma^2[g_{1,2}] = \frac{2}{\Omega_q}\sum_{i,j=1}^{2}(g_i|\mathbf{C}_{ij}|g_j), \tag{56}$$

where correlation functions C_{ij} among the noises are defined as

$$C_{ij}(t,t') \equiv \langle \delta\hat{b}_i(t)\delta\hat{b}_j(t')\rangle_{\rm sym}\,, \quad i,j = 1,2\,. \tag{57}$$

The optimal $g_{1,2}(t)$ that minimize σ^2 can be obtained through the standard constraint variational method. We define an effective functional as

$$\begin{aligned} J_{\rm eff} &= \frac{1}{2}\sum_{i,j}(g_i|\mathbf{C}_{ij}|g_j) - \mu_1(f_1|g_2) - \mu_2(f_2|g_2) \\ &= \frac{1}{2}\sum_{i,j}(g_i|\mathbf{C}_{ij}|g_j) - (\mu_1 f_1 + \mu_2 f_2|g_2), \end{aligned} \tag{58}$$

where μ_1 and μ_2 are Lagrange multipliers due to the constraints in Eq. (49). Requiring the functional derivative of $J_{\rm eff}$ with respect to g_1 and g_2 equal to zero, we obtain

$$\mathbf{C}_{11}|g_1) + \mathbf{C}_{12}|g_2) = 0\,, \tag{59}$$
$$\mathbf{C}_{21}|g_1) + \mathbf{C}_{22}|g_2) = |\mu_1 f_1 + \mu_2 f_2)\,. \tag{60}$$

This leads to

$$|g_1) = -\mathbf{C}_{11}^{-1}\mathbf{C}_{12}|g_2)\,, \tag{61}$$
$$|g_2) = \mathbf{M}|\mu_1 f_1 + \mu_2 f_2)\,, \tag{62}$$

where we have defined

$$\mathbf{M} \equiv \left[\mathbf{C}_{22} - \mathbf{C}_{21}\mathbf{C}_{11}^{-1}\mathbf{C}_{12}\right]^{-1}\,. \tag{63}$$

Re-imposing Eqs. (49), Lagrange multipliers $\mu_{1,2}$ are then related to ζ as

$$\begin{bmatrix} (f_1|\mathbf{M}|f_1) & (f_1|\mathbf{M}|f_2) \\ (f_2|\mathbf{M}|f_1) & (f_2|\mathbf{M}|f_2) \end{bmatrix}\begin{bmatrix}\mu_1\\ \mu_2\end{bmatrix} = \begin{bmatrix}\cos\zeta\\ \sin\zeta\end{bmatrix} \tag{64}$$

which leads to an optimal σ as the following quadratic form:

$$\sigma^2_{\rm opt} = [\cos\zeta\ \ \sin\zeta]\mathbf{V}^{\rm add}\begin{bmatrix}\cos\zeta\\ \sin\zeta\end{bmatrix} \tag{65}$$

where $\mathbf{V}^{\rm add}$ is a 2×2 covariance matrix,

$$\mathbf{V}^{\rm add} = \frac{2}{\Omega_q}\begin{bmatrix} (f_1|\mathbf{M}|f_1) & (f_1|\mathbf{M}|f_2) \\ (f_2|\mathbf{M}|f_1) & (f_2|\mathbf{M}|f_2) \end{bmatrix}^{-1}. \tag{66}$$

Due to the linearity in Eqs. (60) and (64), the optimal $g_{1,2}$ for a given quadrature ζ can also be rewritten formally as

$$g_j^\zeta = g_j^X\cos\zeta + g_j^P\sin\zeta\,, \quad j = 1,2. \tag{67}$$

This again manifests the fact that a sub-Heisenberg tomography requires different measurement setups for different quadratures.

D. Optimal verification scheme and additional noise covariance with Markovian-noise budget

In our case, we assume all the noises ($\hat{a}_i, \hat{n}_i, \hat{\xi}_{\rm F}$ and $\hat{\xi}_{\rm x}$) are Markovian Gaussian processes. They are fully

characterized by two-point correlation functions as given by

$$\langle \hat{a}_i(t)\hat{a}_j(t')\rangle_{\rm sym} = \delta_{ij}e^{\pm 2q}\delta(t-t')/2\,, \quad (68)$$
$$\langle \hat{n}_i(t)\hat{n}_j(t')\rangle_{\rm sym} = \delta_{ij}\delta(t-t')/2, \quad (69)$$
$$\langle \hat{\xi}_F(t)\hat{\xi}_F(t')\rangle_{\rm sym} = S_F^{\rm th}\delta(t-t')/2, \quad (70)$$
$$\langle \hat{\xi}_x(t)\hat{\xi}_x(t')\rangle_{\rm sym} = S_x^{\rm th}\delta(t-t')/2. \quad (71)$$

Therefore, the corresponding correlation functions for the output noise $\delta\hat{b}_i$ are

$$C_{11}(t,t') = \frac{e^{2q}+\eta}{2}\delta(t-t'), \quad (72)$$
$$C_{12}(t,t') = C_{21}(t',t) = \frac{e^{2q}\alpha^2}{2\hbar}G_x(t'-t), \quad (73)$$
$$C_{22}(t,t') = \frac{\Lambda^2}{4}\delta(t-t') + \frac{\alpha^4}{\hbar^2} \left(\frac{e^{2q}}{2}+\zeta_F^2\right)\int_0^\infty dt_1 G_x(t-t_1)G_x(t'-t_1), \quad (74)$$

with $\Lambda \equiv \sqrt{2(e^{-2q}+\eta+2\zeta_x^2)}$. Plugging these C_{ij} into Eq. (61) and (62), we can obtain the equations for the optimal filtering functions g_1 and g_2. Specifically, for g_1, we have

$$g_1(t) + \frac{e^{2q}}{e^{2q}+\eta}\frac{\alpha^2}{\hbar}\int_t^{T_{\rm int}} dt' G_x(t'-t)g_2(t') = 0. \quad (75)$$

For g_2, by writing out $\mathbf{M}$ explicitly, it gives

$$\frac{\Lambda^2}{4}g_2(t) + \zeta_F'^2\frac{\alpha^4}{\hbar^2}\iint_0^{T_{\rm int}} dt'dt_1 G_x(t-t_1)G_x(t'-t_1)g_2(t') = h(t)\,, \quad (76)$$

where we have redefined the ratio between Brownian thermal noise SQL touching frequency Ω_F and Ω_q (i.e. ζ_F) as ζ_F', which is given by

$$\zeta_F' \equiv \left[\frac{e^{2q}\eta}{2(e^{2q}+\eta)}+\zeta_F^2\right]^{1/2} \approx \left[\frac{\eta}{2}+\zeta_F^2\right]^{1/2}. \quad (77)$$

We see that although g_1 is still defined from g_2, the optimal verification strategy does not totally evade the back action, as is manifested in the term proportional to η inside the bracket of Eq. (77). In the limit of no optical loss with $\eta = 0$, it is identical to the BAE condition in Eq. (55) . Typically, we have 1% optical loss $\eta = 0.01$, squeezing $e^{2q} = 10$ and $\zeta_F = 0.2$, this optical loss will only shift ζ_F by 6%, which is negligible. However, if the thermal noise further decreases and/or the measurement strength increases, the effect of optical loss will become significant, entering in a similar way as the frequency-domain variational measurement proposed by Kimble *et al.*.

The above integral equations for g_1 and g_2 can be solved analytically as elaborated in the Appendix, which in turn gives $\mathbf{M}$ and corresponding $\mathbf{V}^{\rm add}$ defined in Eq. (66). In the free-mass limit with $\Omega_q \gg \omega_m$, the high Q-factor oscillator can be well approximated as a free mass. This allows us to obtain closed forms for g_1 and g_2, as given by (cf. Eq. (67))

$$g_1^X = g_1|_{\zeta=0} = (\Omega_q/\chi)\, e^{-\Omega_q\chi t}\sin\Omega_q\chi t; \quad (78)$$
$$g_1^P = g_1|_{\zeta=\frac{\pi}{2}} = -\sqrt{2}\,\Omega_q\, e^{-\Omega_q\chi t}\sin\left(\Omega_q\chi t+\frac{\pi}{4}\right), \quad (79)$$

and

$$g_2^X = g_2|_{\zeta=0} = 2\,\Omega_q\chi\, e^{-\Omega_q\chi t}\cos\Omega_q\chi t; \quad (80)$$
$$g_2^P = g_2|_{\zeta=\frac{\pi}{2}} = 2\sqrt{2}\,\Omega_q\chi^2\, e^{-\Omega_q\chi t}\sin\left(\Omega_q\chi t-\frac{\pi}{4}\right), \quad (81)$$

with $\chi \equiv [\zeta_F'^2/\Lambda]^{1/2}$. The corresponding verification time scale is set by $\tau_V = (\chi\Omega_q)^{-1}$ and $\tau_q < \tau_V < \tau_F$, which recovers the order-of-magnitude estimate in Sec. II D. To illustrate the behavior of the optimal filtering functions, we show $g_{1,2}^{X,P}$ in Fig. 3. As we can see, the verification process finishes after several τ_q, i.e. in a time scale of τ_V.

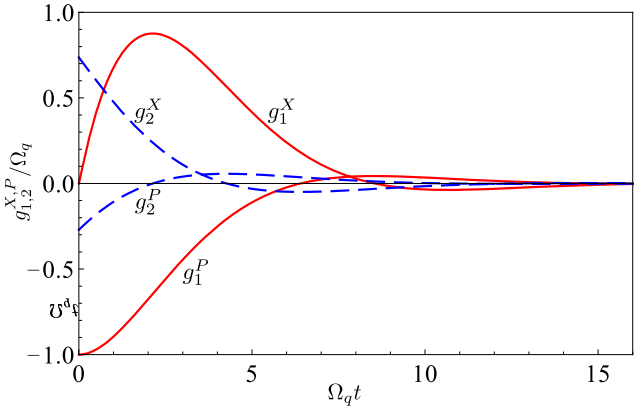

FIG. 3: Optimal filtering functions g_1 (solid curve) and g_2 (dashed curve) in presence of Markovian noise. We have assumed $\Omega_q/2\pi = 100$ Hz, $\zeta_x = \zeta_F = 0.2$, $\eta = 0.01$ and vacuum input ($q = 0$).

The corresponding additional covariance matrix $\mathbf{V}^{\rm add}$ is given by

$$\mathbf{V}^{\rm add} = \begin{bmatrix} \Lambda^{\frac{3}{2}}\zeta_F'^{\frac{1}{2}}\delta x_q^2 & -\Lambda\zeta_F'\hbar/2 \\ -\Lambda\zeta_F'\hbar/2 & 2\Lambda^{\frac{1}{2}}\zeta_F'^{\frac{3}{2}}\delta p_q^2 \end{bmatrix}. \quad (82)$$

A more summarizing measure of the additional noise is the purity, i.e. the area of the additional noise ellipse, measured in units of that for vacuum ellipse,

$$U^{\rm add} \equiv \frac{2}{\hbar}\sqrt{\det\mathbf{V}^{\rm add}} = \Lambda\,\zeta_F'. \quad (83)$$

This simply recovers the order-of-magnitude estimate given in the previous section. In Fig. 4, we show the additional noise ellipse in the case of $\zeta_x = \zeta_F = 0.2$, optical loss $\eta = 1\%$ and with (Green dotted curve) or without (red long-dashed curve) 10 dB input squeezing.

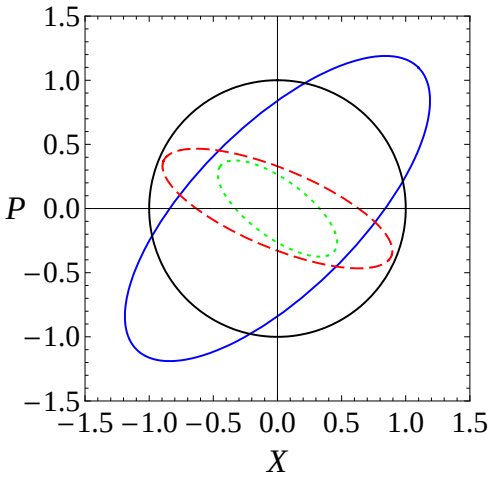

FIG. 4: Additional verification noise ellipse in presence of Markovian noise. We assume $\zeta_x = \zeta_F = 0.2$, vacuum input (Dashed curve), $\zeta_x = \zeta_F = 0.2$ and 10 dB squeezing (Dotted curve). We also show the vacuum level in a unit circle and the ideal conditional quantum state in solid ellipse.

In comparison, we also plot the vacuum level (unit circle) and conditional state obtained through an ideally noiseless state preparation (blue solid ellipse). As figure shows, the least challenging scenario already begins to characterize the conditional state down to the Heisenberg Uncertainty. In this two cases, we have $\Lambda = 1.48$ and 0.62 respectively, leading to

$$U^{\rm add} = 0.30 \text{ (vacuum)}\,, \quad 0.12 \text{ (10 dB squeezing)}. \tag{84}$$

E. Verification after Evolution

To probe the quantum dynamics of the oscillator and the thermal decoherence effect, we can delay the verification for a finite amount of time τ to let the conditional quantum state evolve freely. As mentioned in Sec. III A, the variance will grow due to the back-action and thermal noises. It is essential to evade the back-action imposed during the evolution to achieve a sub-Heisenberg accuracy. Ideally, we can switch off the laser during the interval $(0,\tau)$ to evade the back action. However, this is not easily achievable experimentally due to noise coupling during transient. Instead, during the evolution stage at $(0,\tau)$, we do not measure the phase quadrature $\hat{b}_2$ which contains the information about oscillator position $\hat{x}$, but rather detect the amplitude quadrature $\hat{b}_1$ to record the back-action noise imposed during this period. Mathematically, this can be achieved simply by imposing that $g_2(t) = 0$ at $t < \tau$, namely with the weighted quantity given by

$$\hat{Y} = \int_0^{T_{\rm int}} [g_1(t)\hat{b}_1(t) + \Theta(t-\tau)g_2(t-\tau)\hat{b}_2(t)]. \tag{85}$$

Applying the same formalism as outlined in the previous sections, we can derive CM for the minimal additional noise including evolution to be

$$\mathbf{V}^{\rm add}(\tau) = \begin{bmatrix} V_{xx}^{\rm add} & V_{xp}^{\rm add} \\ V_{px}^{\rm add} & V_{pp}^{\rm add} \end{bmatrix}, \tag{86}$$

where in the free-mass limit,

$$\begin{aligned} V_{xx}^{\rm add} &= [\Lambda^{\frac{3}{2}}{\zeta'_F}^{\frac{1}{2}} + 2\Lambda\zeta'_F\theta + 2\Lambda^{\frac{1}{2}}{\zeta'_F}^{\frac{3}{2}}\theta^2 + (2/3){\zeta'_F}^2\theta^3]\delta x_q^2, \\ V_{xp}^{\rm add} &= V_{px}^{\rm add} = -(\Lambda\zeta'_F + 2\Lambda^{\frac{1}{2}}{\zeta'}^{\frac{3}{2}}\theta + {\zeta'_F}^2\theta^2)\hbar/2, \\ V_{pp}^{\rm add} &= 2(\Lambda^{\frac{1}{2}}{\zeta'_F}^{\frac{3}{2}} + {\zeta'_F}^2\theta)\delta p_q^2, \end{aligned}$$

with dimensionless evolution duration $\theta \equiv \Omega_q\tau$. In Fig. 5, we show the area of the additional noise as a function of τ. As we can see from the figure, with optimal variational measurement we are able to achieve sub-Heisenberg accuracy even after waiting for serval τ_q, which can be applied to verify the quantum dynamics of the oscillator.

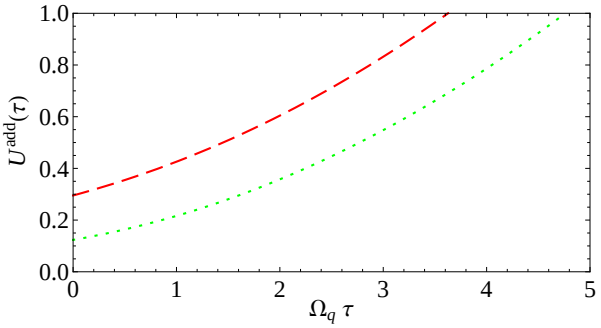

FIG. 5: Area of the additional noise ellipse as a function of evolution duration τ. The specifications and styles are the same as in Fig. 4.

IV. VERIFICATION OF MACROSCOPIC QUANTUM ENTANGLEMENT

In this section, we will apply our protocol in verifying macroscopic entanglement between test masses in GW detector, which was proposed in Refs. [17, 27]. In the experiment as shown schematically in Fig. 6, measurements at the bright and dark port of the interferometer continuously collapse the quantum state of the corresponding common and differential modes of the test-mass motion. This creates two highly squeezed Gaussian state in both modes. Since the common and differential modes are linear combinations of the center of mass motion of the north arm $\hat{x}^{\rm N}$ and the east arm $\hat{x}^{\rm E}$, namely $\hat{x}^{\rm c} = \hat{x}^{\rm E} + \hat{x}^{\rm N}$ and $\hat{x}^{\rm d} = \hat{x}^{\rm E} - \hat{x}^{\rm N}$, this will naturally generate quantum entanglement between the test masses in two arms (e.g. $\rm ITM_N$ and $\rm ITM_E$), which is similar to creating entanglements by mixing two squeezed beams at the beam splitter [28, 29].

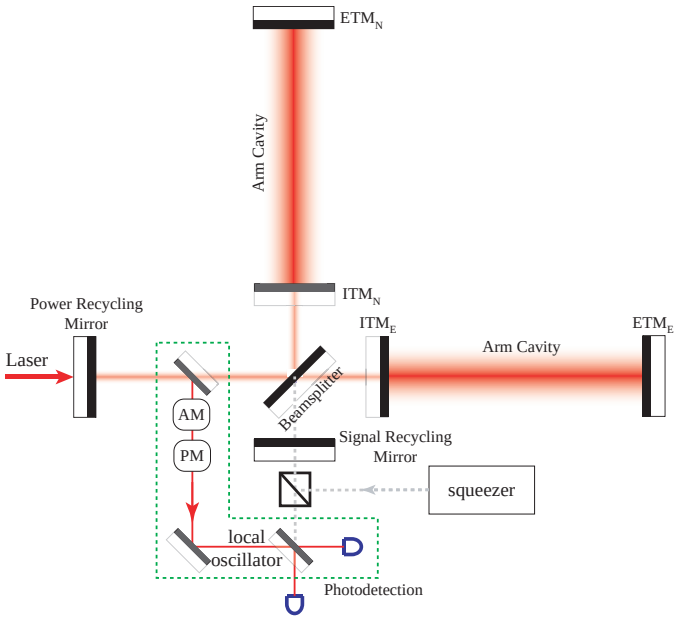

FIG. 6: Advanced GW detectors for macroscopic entanglements between test masses as a test for gravity decoherence. For simplicity, we haven't displayed the setup at the bright port, which is identical to the dark port as shown.

A. Entanglement survival time

To quantify the entanglement strength, we follow Refs. [17, 27] by evaluating the logarithmic negativity defined in Refs. [30, 31]. The bipartite covariances among $(\hat{x}^{\rm E}, \hat{p}^{\rm E}, \hat{x}^{\rm N}, \hat{p}^{\rm N})$ ($\hat{p}_{\rm E,N} \equiv \mu\, \dot{\hat{x}}_{\rm E,N}$ with reduced mass $\mu = m/2$) form the following CM

$$\mathbf{V} = \begin{bmatrix} \mathbf{V}_{\rm EE} & \mathbf{V}_{\rm EN} \\ \mathbf{V}_{\rm NE} & \mathbf{V}_{\rm NN} \end{bmatrix}, \tag{87}$$

where

$$\mathbf{V}_{\rm EE} = \mathbf{V}_{\rm NN} = \begin{bmatrix} (V^{\rm c}_{xx} + V^{\rm d}_{xx})/4 & (V^{\rm c}_{xp} + V^{\rm d}_{xp})/2 \\ (V^{\rm c}_{xp} + V^{\rm d}_{xp})/2 & (V^{\rm c}_{pp} + V^{\rm d}_{pp}) \end{bmatrix}, \tag{88}$$

$$\mathbf{V}_{\rm NE} = \mathbf{V}_{\rm EN} = \begin{bmatrix} (V^{\rm c}_{xx} - V^{\rm d}_{xx})/4 & (V^{\rm c}_{xp} - V^{\rm d}_{xp})/2 \\ (V^{\rm c}_{xp} - V^{\rm d}_{xp})/2 & (V^{\rm c}_{pp} - V^{\rm d}_{pp}) \end{bmatrix}. \tag{89}$$

The logarithmic negativity $E_{\mathcal{N}}$ can then be written as

$$E_{\mathcal{N}} = \max[0, -\log_2 2\sigma_-/\hbar], \tag{90}$$

where $\sigma_- \equiv \sqrt{(\Sigma - \sqrt{\Sigma^2 - 4\det\mathbf{V}})/2}$ and $\Sigma \equiv \det\mathbf{V}_{\rm NN} + \det\mathbf{V}_{\rm EE} - 2\det\mathbf{V}_{\rm NE}$. In contrast to Refs. [17, 27], now the covariance $\mathbf{V}$ corresponds to the total variance $\mathbf{V}^{\rm tot}$ after the entire preparation-verification process. In case of Markovian process, $\mathbf{V}^{\rm tot}$ would simply be a sum of the conditional variance of the prepared quantum state and the added verification noise, namely $\mathbf{V}^{\rm tot} = \mathbf{V}^{\rm cond} + \mathbf{V}^{\rm add}$.

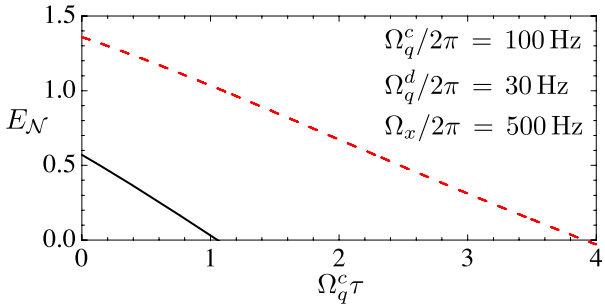

FIG. 7: Logarithmic negative as a function of free-evolution duration, which indicates how long the entanglement survives. The solid curve corresponds to the case where $\Omega_F/2\pi = 20\,\mathrm{Hz}$ and the dashed curve for $\Omega_F/2\pi = 10\,\mathrm{Hz}$. To maximize the entanglement, the common mode is 10 dB phase squeezed at $t > 0$ and $t < 0$ while the differential mode is 10 dB amplitude squeezed at $t < 0$ and switching to 10 dB phase squeezed at $t > 0$.

B. Entanglement Survival as a Test of Gravity Decoherece

In order to investigate the survival of the macroscopic quantum entanglement, we will include the free evolution stage mentioned in the previous section. This can help us to understand whether there is any additional decoherence effects, such as *Gravity decoherence* suggested by Diósi and Penrose [3, 4]. According to their models, quantum superpositions vanishes within a time scale of $\hbar/E_G$. Here E_G can be (a) self-energy of the mass-distribution-difference, namely

$$E_G^{(a)} = \int d\mathbf{x}d\mathbf{y}\, G[\rho(\mathbf{x}) - \rho'(\mathbf{x})][\rho(\mathbf{y}) - \rho'(\mathbf{y})]/r \tag{91}$$

with ρ denoting the mass density distribution and $r \equiv |\mathbf{x} - \mathbf{y}|$; Alternatively, it can be (b) spread of mutual gravitational energy among components of the quantum superposition, namely

$$E_G^{(b)} = \int d\mathbf{x}d\mathbf{y}\, G\rho(\mathbf{x})\rho'(\mathbf{y})\, \delta\mathbf{r}/r^{3/2}. \tag{92}$$

For the prepared test-mass quantum states with width of δx_q, we have

$$\tau_G^{(a)} \approx \Omega_q/(G\rho)\,,\ \tau_G^{(b)} \approx \hbar^{1/2}L^2\Omega_q^{1/2}/(GM^{3/2})\,. \tag{93}$$

where L is the distance between two ITMs, and M is the mass. Plugging the typical values for LIGO mirrors with $\rho = 2.2\,g/\mathrm{cm}^3$, $L \approx 10\,\mathrm{m}$ (ITMs) and $M = 10\,\mathrm{kg}$, we have

$$\tau_G^a = 4.3\times10^9\,\mathrm{s}, \quad \tau_G^b = 1.2\times10^{-5}\,\mathrm{s}. \tag{94}$$

It is therefore quite implausible to test model (a); while for model (b), $\Omega_q\tau_G^{(b)}$ is less 0.01 with $\Omega_q/2\pi = 100$ Hz. In Fig. 7, we show the entanglement survival as a function of evolution duration. As we can see, the model (b) of gravity decoherence can easily be tested, for the entanglement can survive for several times of the measurement

time scale $1/\Omega_q$, which is much longer than the predicted $\tau_G^{(b)}$.

V. CONCLUSIONS

In this paper, we have shown that a two-staged MQM experiment including preparation and verification processes allows to study quantum mechanics of macroscopic objects. We have demonstrated that an optimal time-domain variational measurement can provide a sub-Heisenberg tomography of prepared macroscopic quantum state and a high-accuracy verification of macroscopic quantum entanglements as a test of gravity decoherece. To motivate MQM experiments in future long-baseline interferometric GW detectors, we have been focusing on the relevant free-mass regime where the measurement frequency is much higher than the mechanical frequency. However, techniques described in this paper applies in general cases, such as small-scale experiments which may be able to reach the SQL in a shorter time frame. To this respect, we note that in our results for Markovian systems only depend on the ratio between various noises and the SQL, and therefore carries over directly to systems with other scales. In addition, the Markovian assumption applies more accurately to smaller-scale systems which operate in higher frequencies.

Acknowledgments

We thank all the members of the AEI-Caltech-MIT MQM discussion group for very useful discussions. We thank K. S. Thorne for initiating this research project, and V.B. Braginsky for important critical comments. Research of Y. C., S. D., H. M.-E. and K. S. is supported by the Alexander von Humboldt Foundations Sofja Kovalevskaja Programme, as well as NSF grants PHY-0653653 and PHY-0601459 and the David and Barbara Groce startup fund at Caltech. Research of H. R. is supported by the Deutsche Forschungsgemeinschaft through the SFB No. 407. H. M has been supported by the Australian Research Council and the Department of Education, Science and Training.

APPENDIX A: SOLVING THE INTEGRAL EQUATIONS WITH WIENER-HOPF METHOD

Here we will give the analytical solutions to the integral equations we encountered in obtaining the optimal filtering functions g_1 and g_2. Let's consider the general case with a free evolution stage ($0 < t < \tau$). Given the weighted quantity $\hat{Y}$ in Eq. (85),

$$\hat{Y} = \int_0^{T_{\rm int}} [g_1(t)\hat{b}_1(t) + \Theta(t-\tau) g_2(t-\tau)\hat{b}_2(t)] \qquad \text{(A1)}$$

and following the same steps outlined in the main text, we obtain the integral equations for $g_{1,2}$, written out explicitly as

$$\int_0^{T_{\rm int}} dt' \begin{bmatrix} C_{11}(t,t') & C_{12}(t,t'+\tau) \\ C_{21}(t+\tau,t') & C_{22}(t+\tau,t'+\tau) \end{bmatrix} \begin{bmatrix} g_1(t') \\ g_2(t') \end{bmatrix} = \begin{bmatrix} 0 \\ h(t+\tau) \end{bmatrix}, \qquad \text{(A2)}$$

where $C_{ij}\,(i,j=1,2)$ are given by Eq. (73). Since the optimal filter functions $g_{1,2}(t)$ will automatically cut off at large t after when the thermal noise dominates the variance in the oscillator position, we can extend the integration upper limit $T_{\rm int}$ to ∞. In this way, it allows an analytical solution to $g_{1,2}$ using the Wiener-Hopf method. In the frequency domain, they can be written as

$$[\tilde{S}_{11}\tilde{g}_1]_+ + [\tilde{S}_{12}\, e^{i\Omega\tau}\tilde{g}_2]_+ = 0, \qquad \text{(A3)}$$

$$[\tilde{S}_{21}\, e^{-i\Omega\tau}\tilde{g}_1]_+ + [\tilde{S}_{22}\tilde{g}_2]_+ - \tilde{\Gamma} = e^{-i\Omega\tau}\tilde{h}, \qquad \text{(A4)}$$

$$\tilde{\Gamma} = \beta[\tilde{G}_x e^{-i\Omega\tau}(\tilde{G}_x e^{i\Omega\tau}\tilde{g}_2)_-]_+. \qquad \text{(A5)}$$

where spectral densities $\tilde{S}_{ij}$ are the Fourier transformation of the noise correlations C_{ij} and $\beta \equiv (\alpha^4/\hbar^2)[e^{2q} + 2{\zeta'_F}^2]$; $[\ ]_+$ means taking the causal part of the function inside brackets which only has poles in the lower-half complex plane and $[\ ]_-$ corresponds to taking the anti-causal part which only has poles in the upper-half complex plane. By $[e^{-i\Omega\tau}\tilde{f}(\Omega)]_+$ with $\tau > 0$, we mean

$$[e^{-i\Omega\tau}\tilde{f}(\Omega)]_+ = \sum_k \frac{\mathrm{Res}[e^{-i\Omega\tau}\tilde{f}(\Omega),\ \Omega_k^-]}{(\Omega-\Omega_k)^{\theta_k}} \qquad \text{(A6)}$$

with Ω_k^- denoting poles of $\tilde{f}(\Omega)$ in the lower-half complex plane and θ_k the order of the pole (Similar for $[e^{i\Omega\tau}\tilde{f}(\Omega)]_-$). The single-sided spectral densities $\tilde{S}_{ij}(\Omega)$ are given by

$$\tilde{S}_{11} = e^{2q} + \eta, \qquad \text{(A7)}$$

$$\tilde{S}_{12} = -\frac{e^{2q}\Omega_q^2}{(\Omega+\omega_m-i\gamma_m)(\Omega-\omega_m-i\gamma_m)}, \qquad \text{(A8)}$$

$$\tilde{S}_{21} = \tilde{S}_{12}^*(\Omega), \qquad \text{(A9)}$$

$$\tilde{S}_{22} = \frac{\Lambda^2}{2} + \frac{[e^{2q} + 2{\zeta'_F}^2]\Omega_q^4}{[(\Omega+\omega_m)^2+\gamma_m^2][(\Omega-\omega_m)^2+\gamma_m^2]}. \qquad \text{(A10)}$$

Since $\tilde{S}_{11}$ is only a number, for g_1, we simply have

$$\tilde{g}_1 = -\tilde{S}_{11}^{-1}[\tilde{S}_{12}e^{i\Omega\tau}\tilde{g}_2]_+. \qquad \text{(A11)}$$

In the time-domain, this recovers the result in Eq. (75). Through a spectral factorization

$$\tilde{\psi}_+\tilde{\psi}_- \equiv \tilde{S}_{22} - \tilde{S}_{11}^{-1}\tilde{S}_{12}\tilde{S}_{21} \qquad \text{(A12)}$$

with $\tilde{\psi}_{+(-)}$ denoting the causal (anti-causal) part, we obtain the solution for $\tilde{g}_2$:

$$\tilde{g}_2 = \frac{1}{\tilde{\psi}_+}\left\{\left[e^{-i\Omega\tau}\tilde{h} - \tilde{S}_{11}^{-1}\tilde{S}_{21}e^{-i\Omega\tau}(\tilde{S}_{12}e^{i\Omega\tau}\tilde{g}_2)_- + \tilde{\Gamma}\right]_+ / \tilde{\psi}_-\right\}_+. \qquad \text{(A13)}$$

Plugging $\tilde{\Gamma}$ into the above equation, $\tilde{g}_2$ becomes

$$\tilde{g}_2 = \frac{1}{\tilde{\psi}_+}\left\{\left[e^{-i\Omega\tau}\tilde{h} + \kappa\,\tilde{G}_x e^{-i\Omega\tau}(\tilde{G}_x^* e^{i\Omega\tau}\tilde{g}_2)_-\right]/\tilde{\psi}_-\right\}_+ \tag{A14}$$

with $\kappa \equiv m^2\Omega_q^4 {\zeta'_F}^2$. On the right hand side of the above equation, they only involve values of $\tilde{g}_2$ at those poles of $\tilde{G}_x^*$ in the upper half complex plane. They can be obtained by solving the corresponding algebra equations. Therefore, we obtain the analytical solution to $\tilde{g}_1$ and $\tilde{g}_2$. A simple inverse Fourier transformation gives $g_1(t)$ and $g_2(t)$, from which we can derive the CM $\mathbf{V}^{\rm add}(\tau)$ for the added noise. As long as the evolution duration τ is not much longer than the measurement time scale $\sim 1/\Omega_q$, in the free-mass limit where $\Omega_q \gg \omega_m$, we can expand $\mathbf{V}^{\rm add}(\tau)$ as series of $\omega_m\tau \ll 1$, as we have written out explicitly in Eq. (86).

[1] H. J. Kimble,Y. Levin, A. B. Matsko, K. S. Thorne, and Sergey P. Vyatchanin, Phys. Rev. D **65** 022002 (2001); P. Purdue, Phys. Rev. D **66**, 022001 (2002); P. Purdue and Y. Chen, Phys. Rev. D **66**, 122004 (2002).

[2] S. P. Vyatchanin and A. B. Matsko, JETP **77**, 218 (1993); S. P. Vyatchanin and E. A. Zubova, Phys. Lett. A **203**, 269 (1995); S. P. Vyatchanin, ibid. **239**, 201 (1998); S. P. Vyatchanin and A. B. Matsko, JETP **82**, 1007 (1996); S. P. Vyatchanin and A. B. Matsko, JETP **83**, 690 (1996).

[3] L. Diósi, Phys. Lett. A **120** 377 (1987); Phys. Rev. A **40** 1165; J. Phys. A: Math. Theor. **40** 2989 (2007).

[4] R. Penrose, Gen. Rel. Grav. **28** 581 (1996); Phil. Trans. R. Soc. Lond. A **356** 1927; *The Road to Reality: A Complete Guide to the Laws of the Universe*, Alfred A. Knopf, (2005).

[5] P. F. Cohadon and A. Heidmann and M. Pinard, Phys. Rev. Lett. **83**, 3174 (1999).

[6] A. Hopkins, K. Jacobs, S. Habib, and K. Schwab, Phys. Rev. B **68**, 235328 (2003).

[7] D. Kleckner and D. Bouwmeester, Nature **444**, 75 (2006).

[8] T. Corbitt, C. Wipf, T. Bodiya, D. Ottaway, D. Sigg, N. Smith, S. Whitcomb, and N. Mavalvala, Phys. Rev. Lett. **99**, 160801 (2007).

[9] C. M. Mow-Lowry, A. J. Mullavey, S. Gossler, M. B. Gray, and D. E. McClelland, Phys. Rev. Lett. **100**, 010801 (2008).

[10] A. Vinante, M. Bignotto, M. Bonaldi, M. Cerdonio, L. Conti, P. Falferi, N. Liguori, S. Longo, R. Mezzena, A. Ortolan, et al., Phys. Rev. Lett. **101**, 033601 (2008).

[11] B. Abbott et al., submitted to New Journal of Physics (2008).

[12] A. Barchielli, Int. J. Theor. Phys. **32**, 2221 (1992).

[13] C. W. Gardiner and P. Zoller, *Quantum noise* (Springer-Verlag, Berlin, 2004), 3rd ed.

[14] G. J. Milburn, Quantum Semiclass. Opt. **8**, 269 (1996).

[15] A. C. Doherty, S. M. Tan, A. S. Parkins, and D. F. Walls, Phys. Rev. A **60**, 2380 (1999).

[16] H. Mueller-Ebhardt, H. Rehbein, R. Schnabel, K. Danzmann, and Y. Chen, Phys. Rev. Lett. **100**, 013601 (2008).

[17] H. Müller-Ebhardt, H. Rehbein, C. Li, Y. Mino, K. Somiya, R. Schnabel, K. Danzmann, and Y. Chen, *State preparation and macroscopic entanglement in gravitational-wave detectors,* submited to Phys. Rev. A (2009).

[18] http://www.ligo.caltech.edu/advLIGO.

[19] S. Miyoki, T. Uchiyama, K. Yamamoto, H. Hayakawa, K. Kasahara, H. Ishitsuka, M. Ohashi, K. Kuroda, and D. Tatsumi, Class. Quantum Grav. **21**, 1173 (2004).

[20] V. B. Braginsky, JETP **26**, 831 (1968).

[21] C. M. Caves, K. S. Thorne, R. W. Drever, V. D. Sandberg, and M. Zimmermann, Rev. Mod. Phys. **52**, 341 (1980).

[22] V. B. Braginsky and F. Y. Khalili, *Quantum Measurement* (Cambridge University Press, 1992).

[23] Y. Chen *et al.*, in preparaion.

[24] F.Ya. Khalili *et al.*, in preparation.

[25] K. J. Blow, R. Loudon, S. J. D. Phoenix and T. J. Shepherd, Phys. Rev. A **42**, 4102 (1990).

[26] A. Buonanno, Y. Chen and N. Mavalvala, Phys. Rev. D **67**, 122005 (2003).

[27] H. Müller-Ebhardt, H. Rehbein, R. Schnabel, K. Danzmann, and Y. Chen, Phys. Rev. Letts. **100**, 013601 (2008).

[28] A. Furusawa, J. L. Sørensen, S. L. Braunstein, C. A. Fuchs, H. J. Kimble, E. S. Polzik, Science **282**, 706 (1998).

[29] W. P. Bowen, R. Schnabel, P. K. Lam and T. C. Ralph, Phys. Rev. Lett. **90**, 043601 (2003).

[30] G. Vidal and R. F. Werner, Phys. Rev. A **65**, 032314 (2002).

[31] G. Adesso, A. Serafini and F. Illuminati, Phys. Rev. A **70**, 022318 (2004).